# Reconstruction of limited-angle and few-view nano-CT image via total variation iterative reconstruction

Zhiting Liang, Yong Guan, Gang Liu, Rui Bian, Xiaobo Zhang, Ying Xiong, Yangchao Tian*
National Synchrotron Radiation Laboratory, University of Science and Technology of China, Hefei, Anhui 230029, China

## ABSTRACT

Nano-CT has been considered as an important technique applied in analyzing inner-structures of nanomaterials and biological cell. However, maximum rotation angle of the sample stage is limited by sample space; meanwhile, the scan time is exorbitantly large to get enough projections in some cases. Therefore, it is difficult to acquire nano-CT images with high quality by using conventional Fourier reconstruction methods based on limited-angle or few-view projections. In this paper, we utilized the total variation (TV) iterative reconstruction to carry out numerical image and nano-CT image reconstruction with limited-angle and few-view data. The results indicated that better quality images had been achieved.

**Keywords:** nano-CT, TV minimization, MLS-OS-SART-TV, limited-angle image reconstruction

## 1. INTRODUCTION

With the development of synchrotron radiation light sources and the micro- and nano-fabrication technology, high resolution X-ray microscope has been rapidly developed in the past two decades. The images with the resolution of 15nm had been acquired [1] in the Advanced Light Source. Recently, Lawrence Berkeley National Laboratory claimed a record spatial resolution of 10 nm by using soft X-ray scanning and full-field microscope[2]. Nano-CT as a useful tool has been widely used for making the research in the fields of innovative nanoscience, such as nanomagnetic materials [3], environmental sciences [4], materials science [5] and biological science [6].

A full-field transmission hard X-ray microscope has been established at the National Synchrotron Radiation Laboratory (NSRL) [7]. Several significant works based on nano-CT have been reported in nano-materials[8], such as the three-dimensional microstructure of SOFC [9-12], eukaryote cell [13-15], ZnO [16] etc. Although, Nano-CT has achieved many positive results, there are still two key aspects that would influence the quality of the experimental results by using nano-CT. One is the maximum rotation angle of the sample stage which is limited for biological samples imaging, because the sample holder impedes the X-ray when the angle is larger than 75° or less than -75°. The other is the total scan time which is usually over 10 hours due to the lower photon flux from the second generation synchrotron radiation light source. Long exposure time would result in serious noise pollution and the distribution of light intensity varying in the sample surface. While exposure time per view is limited by physical conditions, such as beam intensity, the total number of views should be limited to reduce the entire scan time.

In computed tomography (CT), there are two kinds of principal algorithms for image reconstruction. One is Fourier methods, such as the filtered back-projection (FBP), the other is iterative reconstruction methods, such as the algebraic reconstruction technique (ART) and the simultaneous algebraic reconstruction technique (SART). Fourier methods have been the favored choice by many CT manufacturers due to their lightweight computational burden [17, 18]. Nevertheless, when dealing with a noisy, dynamic, or limited number or angle of projection data, Fourier methods tend to produce poor results.

During the last decade, a constraint of minimizing the TV has been widely used to improve image reconstruction quality. The TV of an image is a numerical quantity reflecting the intensity of the image local changing. This quality benefits TV-based methods in reducing artifacts and improving signal-to-noise ratio signally compared with conventional FBP methods, when an image is reconstructed from few views or limited-angle data [19-22].

*ychtian@ustc.edu.cn Tel: +86-551-3601844 Fax: +86-551-5141078

X-Ray Nanoimaging: Instruments and Methods, edited by Barry Lai, Proc. of SPIE Vol. 8851, 885113

In this paper, we modified the TV-based algorithm and applied it to limited-angle and few-view nano-CT data reconstruction. The Shepp-Logan phantom was used as an example to test the algorithm in different situations, such as sufficient projection data, sufficient projection containing noise, limited-angle and few-view projection data and limited-angle and few-view projection data containing noise. Finally, a slice of yeast cell was reconstructed from limited-angle and few-view projections, which was an implemented instance of the nano-CT.

## 2. TV-BASED ITERATIVE RECONSTRUCTION ALGORITHM

### 2.1 Imaging model

We model CT system as follows:

$$WX = Y \tag{1}$$

Where $Y = [y_1, y_2, \mathrm{L}\ , y_M]^T \in R^M$ is the measured projection data, which mingles with noise. It is impossible to separate them completely. $X = [x_1, x_2, \mathrm{L}\ , x_N]^T \in R^N$ is the unknown image, $W = [w_{i,j}]_{M \times N}$ is an M × N weight matrix, $w_{i,j}$ can be interpreted as the contribution of the $j^{th}$ pixel to the $i^{th}$ ray integral.

### 2.2 Iterative reconstruction

The reconstruction problem is to estimate the unknown image X from projections Y and system matrix W. Generally, the system matrix W is under-determined. The TV minimization has been considered as an effective measure in obtaining high quality reconstructed images from insufficient projections [19-21]. TV-based methods can be defined as [19]:

$$\min \|X\|_{TV}, \quad s.t. \quad WX = Y \tag{2}$$

Where TV is the $l_1$-norm of the gradient image, it is defined as:

$$\|X\|_{\mathrm{TV}} = \sum_{m,n} \sqrt{(X(m+1,n) - X(m,n))^2 + (X(m,n+1) - X(m,n))^2} \tag{3}$$

Sidky et al. have described the projection on convex sets with total variation (POCS-TV) algorithm in detail [19]. Because the ordered subsets-SART (OS-SART) [23] can effectively reduce artifacts and accelerate the convergence, we employed OS-SART instead of ART.

The OS-SART defined by Ge Wang is applied here [23]:

$$x_j^{(kT+t+1)} = x_j^{(kT+t)} + \lambda_k \frac{1}{w_{+j}} \sum_{i \in B_{[t]}} w_{ij} \frac{y_i - W_i x^{(k)}}{w_{i+}}, \quad j = 1,2,\mathrm{L}\ , N \tag{4}$$

where k denotes the iteration number, T indicates the number of the total subsets, t is the current subset's number, $x_j^{(k)}$, $y_i$ and $w_{ij}$ are the same as described in formula one, $\lambda_k$ is the $k^{th}$ relaxation factor, $B_{[t]}$ represents the $t^{th}$ ordered subset, $w_{+j}$ is the sum of the $j^{th}$ pixel contribution to the projections which belong to the $t^{th}$ subset, and $w_{i+}$ is the total contribution of the image to the $i^{th}$ projection. They are defined as follows:

$$w_{+j} = \sum_{i \in B_{[k]}} w_{ij} \neq 0\ , j = 1,2,\mathrm{L}\ , N \ ; \ w_{i+} = \sum_{j=1}^{N} w_{ij} \neq 0\ , i = 1,2,\mathrm{L}\ , M \tag{5}$$

each iteration of the OS-SART-TV algorithm consists of OS-SART and TV minimization. And we skip the positivity constraint for some cases images containing negative values.

Due to the total scan time which is usually over 10 hours, light spot may be not always stable. And some of the noise varies along with the time. The adjacent projections are divided into different subsets in order to balance the noise and

other influence. The index set of the projections is realigned according to the multilevel access scheme (MLS)[24]. Even though the number of views is not a power of two as literature [24] required, we can also use it by decreasing the sampling number in the last level. Then, projections are divided uniformly into L nonempty subsets (in this case, some subsets contain one less view than others). In this paper, the algorithm is addressed as MLS-OS-SART-TV. Fig.1 shows an overview of the MLS-OS-SART-TV algorithm.

**Input:** projections $Y$ and projections' angle
**Algorithm:**
Initialize relaxation parameter $\lambda_k$ ; using the FBP algorithm to get the initial image $X$; realigning the index set deferring to the MLS, and dividing the index set into $L$ nonempty subsets.
$k = 0$;
**while** (step criterion is not met) **do**
**begin**
$k = k+1$;
**for** $t = 1 : L$
$x_j^{(kT+t+1)} = \text{MLS-OS-SART}\ (x_j^{(kT+t)})$
**end**
**for** $q = 1 : Q$
$X^{(kT,q+1)} = \text{TV}\ (X^{(kT,q)})$
**end**
**end**
**Output:** $Y$

Fig.1. Basic steps of the MLS-OS-SART-TV algorithm.

## 3. SIMULATION RESULTS AND DISCUSSION

### 3.1 Numerical phantom data reconstruction

Here, we aim at applying the TV-based iterative reconstruction algorithm to carry out the reconstruction of the limited-angle and few-view data that is acquired from the nano-CT experimental system. To estimate the performance of the TV-based algorithm, the Shepp-Logan phantom is used to test the algorithm under different situations. Fig.2a shows the noise-free Shepp-Logan phantom, and the line profile across the central row of the phantom is presented in Fig.2b. The phantom has 256 × 256 pixels, and the gray level is set between 0 and 1.

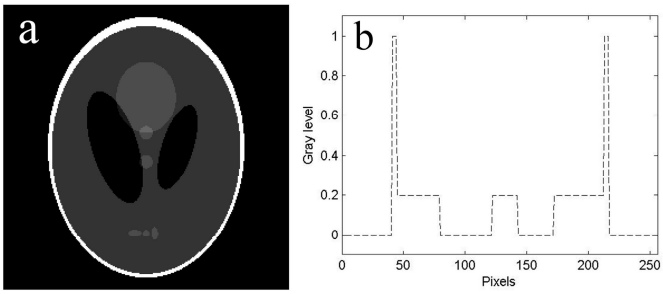


Fig.2. (a) The noise-free Shepp-Logan phantom, (b) the line profile through the central row of the phantom.

Fig.3 shows the reconstructed imaging and line profiles which are reconstructed from the sufficient projection data by the FBP and the MLS-OS-SART-TV algorithm. The FBP reconstruction imaging reconstructed from 180 noise-free projections is shown in Fig.3a, and the line profile is shown in the Fig.3g. With the increase of Poisson noise, severe artifacts are clearly visible in Fig.3b and c, and the line profiles' fluctuation is also more intense and obvious in Fig.3h and i. It illustrates that the FBP reconstruction imaging is not smooth. However, The MLS-OS-SART-TV provides better reconstruction quality when the projections are sufficient and noise-free as shown in Fig.3d, and Fig.3j shows that the

line profile matches well with that of the original phantom. When the noise increases to 5%, the quality of the MLS-OS-SART-TV reconstruction imaging is still good enough. The line profile of the imaging is very smooth as shown in Fig.3k. Even though 10% Poisson noise is added to the projections, non-artifacts can be clearly visible in Fig.3f, and its line profile in Fig.3l is as good as that in Fig.3g.

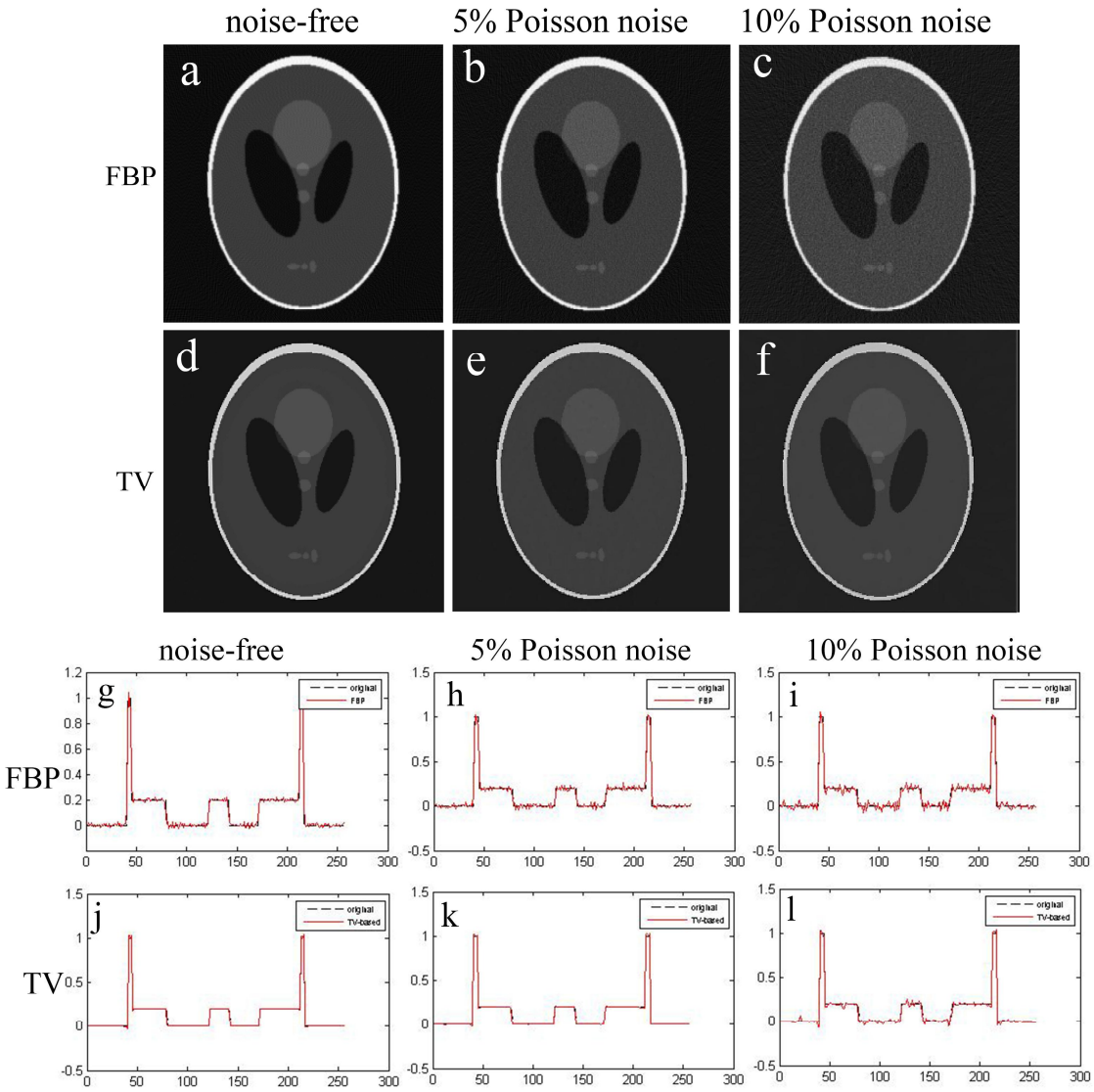


Fig.3. 180 views reconstructed from noise-free and contained Poisson noise projections by the FBP (the first row) and by the MLS-OS-SART-TV algorithm (the second row); (g-l) are line profiles through the central row of (a-f) reconstructions.

Due to long scan time for each projection and to reduce the radiation dose, few-view projections for nano-CT reconstruction are collected. Normally, the angle range is limited to -74° to 74°, and a series of 75 radiographs are collected at angles ranging from −74° to +74° at the intervals of 2°. Fig.4 shows the reconstructed imaging and line profiles which are reconstructed from the 75 projection data by the FBP and the MLS-OS-SART-TV algorithm. Whether the projections contain noise, the reconstruction of the FBP applied in limited-angle and few-view projections is unperfected, and significant artifacts can be visible in Fig.4a and b. The line profiles across the central row of the reconstructions fluctuate intensely as shown in Fig.4e and f. Overall, the FBP algorithms are not suitable for

reconstructing limited-angle and few-view projections. Nevertheless, Fig.4c and d show that the reconstructions of the MLS-OS-SART-TV algorithm are smooth, and only a few of artifacts which are caused by the missing wedge of the projections can be visible at the outside ring. And the inside of the reconstructions match well with the original phantom as shown in Fig.4g and h.

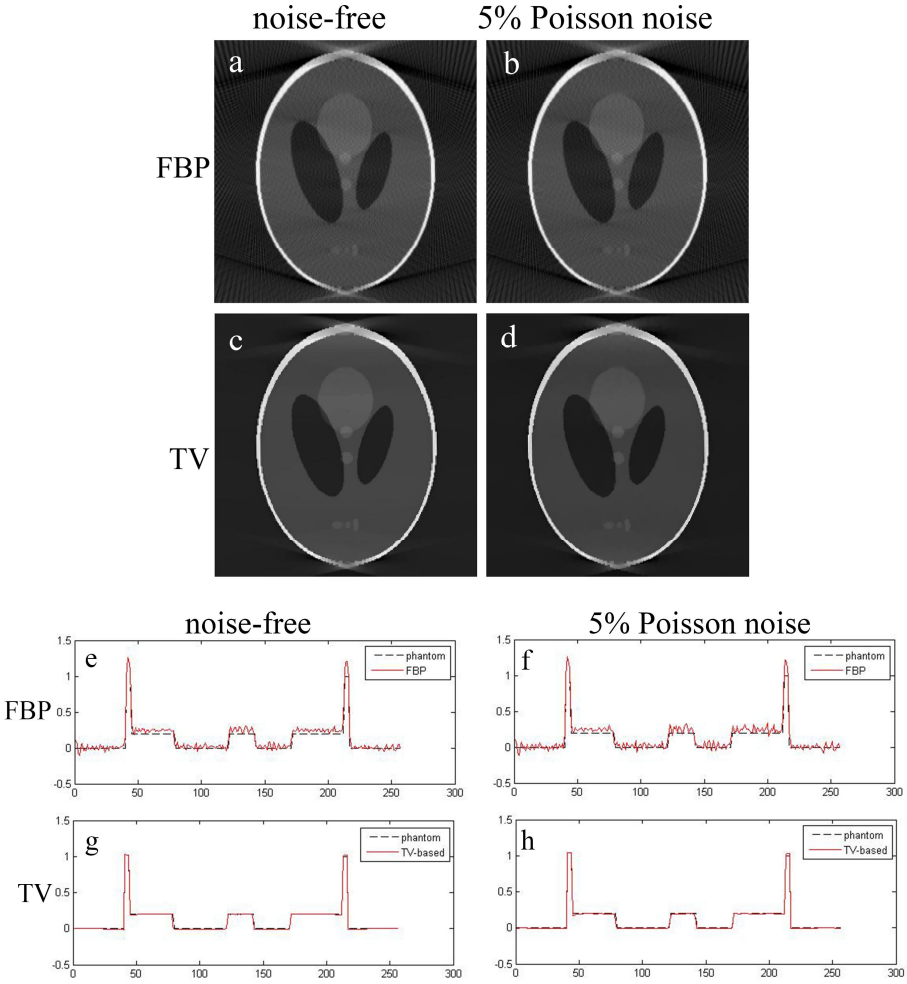


Fig.4. View range limited at -74°:2:74°, imaging reconstructed from noise-free and contained 5% Poisson noise projections by the FBP (a and b) and by the MLS-OS-SART-TV algorithm (c and d); line profiles (e-h) through the central row of the reconstructions (a-d).

### 3.2 Nano-CT phantom reconstruction

One of projections of a yeast cell collected from the nano-CT at the NSRL is shown in Fig.5a. Because the maximum rotation angle of the sample stage is limited for biological samples imaging, the range of the rotation angle is from -74° to 74°. Thus, 75 projections are finally collected. The FBP reconstruction contains many artifacts as shown in the Fig.5b. It is difficult to differentiate the boundary of the cell organelles, and the reconstruction imaging fluctuates intensely as shown in Fig.5b. Fig.5c is a reconstruction of the MLS-OS-SART-TV. The quality of Fig.5c is much better than that of the b. Image artifacts caused by the missing wedge are labeled by the red circles as shown in Fig.5b and c. Because the cell was preprocessed by heavy metal staining, only two groups of organelles based on their obvious difference in X-ray contrast can be observed. And, we can clearly distinguish two groups of organelles through the slice of the yeast cell in Fig.5c. The blue (left) arrow label indicates the organelles with lower X-ray contrast than cytoplasm, whereas the higher X-ray contrast organelles are labeled by the green (right) arrow label as shown in Fig.5b and c.

Thus FBP is not a suitable technique for a noisy, or limited-angle and few-view projection data, and the FBP reconstructions contain too much noise. It can be found that the MLS-OS-SART-TV for limited-angle and few-view projection data is better than FBP.

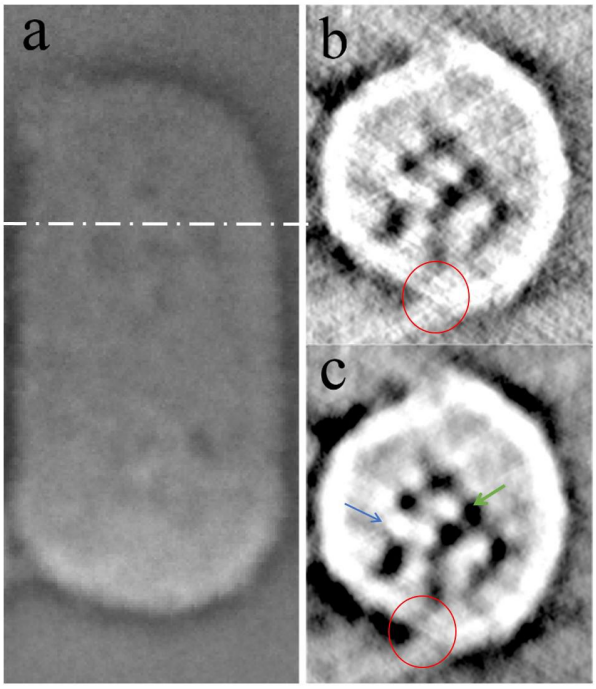


Fig.5. Yeast cell got from Nano-CT. (a) A projection image of the cell; (b) a slice of the cell reconstructed by the FBP; (c) a slice of the cell reconstructed by the MLS-OS-SART-TV algorithm. (b) and (c) are slices along the white imaginary line in (a).

## 4. CONCLUSIONS

Nano-CT, such as transmission hard X-ray microscope, is an important imaging technology for 3D reconstruction of nanostructure and biological samples. However, due to the insufficiency and noisy of the projections, satisfying reconstructions of some biological samples cannot be acquired by conventional Fourier reconstruction methods. In this paper, a TV-based algorithm named MLS-OS-SART-TV was used to reconstruct limited-angle and few-view projections of nano-CT. Firstly, sufficient projections of the Shepp-Logan phantom under various situations were employed to test. The results shown that the MLS-OS-SART-TV algorithm had accurate performance, whether the projections were noise-free or contained Poisson noise. The MLS-OS-SART-TV also had better performance than the FBP when projections were limited-angle and few-view. Finally, the image of yeast cell, which was a typical representative of biological specimens, was captured from nano-CT. It also indicated that the MLS-OS-SART-TV algorithm outperformed the FBP. However, not all of the data of nano-CT are suitable for TV-based algorithm. Only the material that is locally smooth meets the requirements of TV minimization. Some materials with complex structures, for instance the microstructure of a solid-oxide fuel cell anode collected from nano-CT cannot be reconstructed by TV-based algorithm. In future, we will develop a wavelet-based algorithm which is suitable for reconstructing the material with complex structures.

## 5. ACKNOWLEDGMENTS

This work was supported by grants from the 985 project of the State Ministry of Education, the National Natural Science Foundation of China (No. 11275204), the Knowledge Innovation Program of the Chinese Academy of Sciences (KJCX2-YW-N43), the Fundamental Research Funds for the Central Universities (No. WK2310000034), the Major State Basic Research Development Program of China (973 Program) (No. 2012CB825804) and Ph.D. Programs Foundation of Ministry of Education of China (No. 2012340213002).

## REFERENCES


[1] W. L. Chao, B. D. Harteneck, J. A. Liddle *et al.*, "Soft X-ray microscopy at a spatial resolution better than 15nm," Nature, 435(7046), 1210-1213 (2005).

[2] W. Chao, "Real space soft x-ray imaging at 10 nm spatial resolution," (2012).

[3] G. Denbeaux, E. Anderson, W. Chao *et al.*, "Soft X-ray microscopy to 25 nm with applications to biology and magnetic materials," Nuclear Instruments & Methods In Physics Research Section a-Accelerators Spectrometers Detectors And Associated Equipment, 467, 841-844 (2001).

[4] C. Patty, B. Barnett, B. Mooney *et al.*, "Using X-ray Microscopy and Hg L-3 XAMES To Study Hg Binding in the Rhizosphere of Spartina Cordgrass," Environmental Science & Technology, 43(19), 7397-7402 (2009).

[5] P. A. Midgley, E. P. Ward, A. B. Hungria *et al.*, "Nanotomography in the chemical, biological and materials sciences," Chem Soc Rev, 36(9), 1477-94 (2007).

[6] M. Uchida, G. McDermott, M. Wetzler *et al.*, "Soft X-ray tomography of phenotypic switching and the cellular response to antifungal peptoids in Candida albicans," Proc Natl Acad Sci U S A, 106(46), 19375-80 (2009).

[7] Y. C. Tian, W. J. Li, J. Chen *et al.*, "High resolution hard x-ray microscope on a second generation synchrotron source," Review Of Scientific Instruments, 79(10), (2008).

[8] J. Chen, C. Wu, J. Tian *et al.*, "Three-dimensional imaging of a complex concaved cuboctahedron copper sulfide crystal by x-ray nanotomography," Applied Physics Letters, 92(23), 233104 (2008).

[9] Y. Guan, W. Li, Y. Gong *et al.*, "The study of the reconstructed three-dimensional structure of a solid-oxide fuel-cell cathode by X-ray nanotomography," J Synchrotron Radiat, 17(6), 782-5 (2010).

[10] Y. Guan, Y. Gong, W. Li *et al.*, "Quantitative analysis of micro structural and conductivity evolution of Ni-YSZ anodes during thermal cycling based on nano-computed tomography," Journal of Power Sources, 196(24), 10601-10605 (2011).

[11] Y. Guan, W. Li, Y. Gong *et al.*, "Analysis of the three-dimensional microstructure of a solid-oxide fuel cell anode using nano X-ray tomography," Journal of Power Sources, 196(4), 1915-1919 (2011).

[12] Y. Guan, Y. Gong, G. Liu *et al.*, "Analysis of impact of sintering time on microstructure of LSM-YSZ composite cathodes by X-ray nanotomography," Materials Express, 3(2), 166-170 (2013).

[13] J. Chen, Y. Yang, X. Zhang *et al.*, "3D nanoscale imaging of the yeast, Schizosaccharomyces pombe, by full-field transmission X-ray microscopy at 5.4 keV," Anal Bioanal Chem, 397(6), 2117-21 (2010).

[14] Y. Yang, W. Li, G. Liu *et al.*, "3D visualization of subcellular structures of Schizosaccharomyces pombe by hard X-ray tomography," J Microsc, 240(1), 14-20 (2010).

[15] T. Zheng, W. Li, Y. Guan *et al.*, "Quantitative 3D imaging of yeast by hard X-ray tomography," Microsc Res Tech, 75(5), 662-6 (2012).

[16] W. Li, N. Wang, J. Chen *et al.*, "Quantitative study of interior nanostructure in hollow zinc oxide particles on the basis of nondestructive x-ray nanotomography," Applied Physics Letters, 95(5), 053108 (2009).

[17] K. Mueller, R. Yagel, and J. J. Wheller, "Anti-aliased three-dimensional cone-beam reconstruction of low-contrast objects with algebraic methods," Medical Imaging, IEEE Transactions on, 18(6), 519-537 (1999).

[18] G. L. Zeng, [Medical image reconstruction: A conceptual Tutorial] Springer, (2010).

[19] E. Y. Sidky, C.-M. K. a. o, and X. c. P. n, "Accurate image reconstruction from few-views and limited-angle data in divergent-beam CT," Journal of X-Ray Science and Technology, (2006).

[20] J. Velikina, S. Leng, and G. H. Chen, "Limited view angle tomographic image reconstruction via total variation minimization," Medical Imaging 2007: Physics of Medical Imaging, Pts 1-3, 6510, U1044-U1055 (2007).

[21] V. P. Gopi, and P. Palanisamy, "CT image reconstruction based on combination of iterative reconstruction technique and total variation." 49-52.

[22] S. J. LaRoque, E. Y. Sidky, and X. C. Pan, "Image reconstruction from sparse data samples along spiral trajectories in MRI," Medical Imaging 2007: Physics of Medical Imaging, Pts 1-3, 6510, U1977-U1982 (2007).

[23] G. Wang, and M. Jiang, "Ordered-subset simultaneous algebraic reconstruction techniques (OS-SART)," Journal Of X-Ray Science And Technology, 12(3), 169-177 (2004).

[24] H. Guan, and R. Gordon, "A projection access order for speedy convergence of ART (algebraic reconstruction technique): a multilevel scheme for computed tomography," Phys Med Biol, 39(11), 2005-22 (1994).